Palaeogeography, Palaeoclimatology, Palaeoecology 506 (2018) 12–21

Contents lists available at ScienceDirect

Palaeogeography, Palaeoclimatology, Palaeoecology

journal homepage: www.elsevier.com/locate/palaeo

Primary productivity in the western tropical Atlantic follows Neogene Amazon River evolution

E.I. Lammertsma[a,b,*], S.R. Troelstra[c,d], J.-A. Flores[e], F. Sangiorgi[f], F. Chemale Jr.[b], D.A. do Carmo[b], C. Hoorn[a]

[a] Institute for Biodiversity and Ecosystem Dynamics (IBED), University of Amsterdam, P.O. Box 94248, 1090 GE Amsterdam, the Netherlands
[b] Institute of Geosciences, University of Brasília, Federal District, 70297-400 Brasília, DF, Brazil
[c] Cluster Earth and Climate, VU University Amsterdam, De Boelelaan 1085, 1081 HV Amsterdam, the Netherlands
[d] NBC Naturalis, Darwinweg 2, 2333 CR Leiden, the Netherlands
[e] Department of Geology, Grupo de Geociencias Oceánicas, Universidad de Salamanca, Casa del Bedel, Cardenal Plá y Deniel, 22, Planta baja, 37008 Salamanca, Spain
[f] Department of Earth Sciences, Marine Palynology and Paleoceanography, Utrecht University, Princetonlaan 8a, 3584 CB Utrecht, the Netherlands

ARTICLE INFO

Keywords:
Amazon Fan
Brazilian Equatorial Margin
Neogene
Foraminifera
Organic-walled dinoflagellate cysts

ABSTRACT

The Amazon River nutrient-rich plume currently triggers large-scale phytoplankton blooms in the otherwise oligotrophic western tropical Atlantic Ocean. Little is known about the onset and development of this high productivity system, although a direct link to the transcontinental Amazon River evolution can be expected. The Amazon submarine fan, located on the Brazilian Equatorial Margin (BEM), contains a unique sediment archive of the river's history and associated environmental changes in the marine realm. This study represents the first marine microfossil multi-proxy approach applied to any sedimentary record in the submarine fan area for the time interval encompassing the onset and development of the transcontinental Amazon River system. To reconstruct Miocene to Pleistocene changes in surface- and bottom water conditions we analyzed organic-walled dinoflagellate cyst- and benthic foraminiferal assemblages, respectively. Moreover, terrestrial- and freshwater palynomorph abundances were studied to provide a link between fluvial input and marine environmental changes. In addition, a planktonic foraminiferal biostratigraphy is constructed to verify the available calcareous nannofossil-based age model. Our data show that in the early- mid Miocene up to ~13 Ma limited fluvial input reached the BEM and primary productivity was elevated, after which distinctly low productivity conditions prevailed. After the birth of the transcontinental Amazon at ~9 Ma surface water productivity initially increased slightly. Consistently high surface water productivity and decreased bottom water oxygenation followed increasing terrestrial input after the (early) Pliocene. The temporal consistency between records from the Amazon Fan and the more distant Ceará Rise reflects large-scale marine environmental changes followed the development of the Amazon River, likely related to increased climatic variability in the Amazon Basin during the Plio-Pleistocene.

1. Introduction

When viewing the western tropical Atlantic Ocean (WTA) from space, a curved ribbon of dark colored water can be traced from the mouth of the Amazon River (Brazil) northward along the shore and into the otherwise clear ocean: the Amazon Plume. With an annual discharge exceeding 6600 km^3 per year, the Amazon River delivers ~20% of the global fluvial input to the oceans (Dai and Trenberth, 2002). The low-saline plume water is rich in inorganic- and organic suspended particles as well as transparent- and colored dissolved organic matter, the latter determining the striking discoloration of the offshore plume (e.g. Del Vecchio and Subramaniam, 2004; Hu et al., 2004; Salisbury et al., 2011). Driven by seasonal migration of the Intertropical Convergence Zone (ITCZ), oceanic boundary currents transport the Amazon water north towards the Caribbean Sea in boreal winter, and also eastward across the Atlantic Ocean from May to October (Fig. 1; e.g. Coles et al., 2013; Hu et al., 2004; Muller-Karger et al., 1988), covering an area of up to 2×10^6 km^2 (Körtzinger, 2003). In short, the Amazon Plume creates spatially and seasonally variable high-nutrient and lower-salinity conditions of unique magnitude in the otherwise oligotrophic WTA.

Phytoplankton profits from the fluvial dissolved organic matter- and

* Corresponding author at: Institute for Biodiversity and Ecosystem Dynamics (IBED), University of Amsterdam, P.O. Box 94248, 1090 GE Amsterdam, the Netherlands.
E-mail addresses: emmylam@gmail.com (E.I. Lammertsma), s.r.troelstra@vu.nl (S.R. Troelstra), flores@usal.es (J.-A. Flores), f.sangiorgi@uu.nl (F. Sangiorgi), faridcj@unisinos.br (F. Chemale Jr.), delei1998@gmail.com (D.A. do Carmo), m.c.hoorn@uva.nl (C. Hoorn).

https://doi.org/10.1016/j.palaeo.2018.05.048
Received 8 December 2017; Received in revised form 6 May 2018; Accepted 30 May 2018
Available online 06 June 2018
0031-0182/

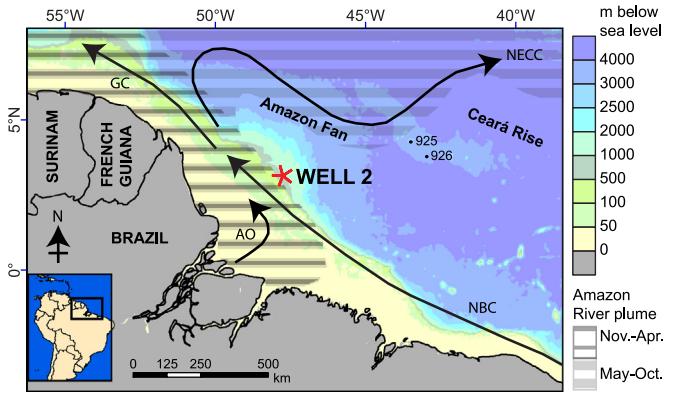

Fig. 1. Map with bathymetry of the Brazilian Equatorial Margin, Amazon Fan and Ceará Rise (including drill site locations). Well 2 (3°2′58.660″N; 47°44′45.801″W) is located at a water depth of 754 m. The present-day approximate seasonal extent of the river plume (grey shading) is based on Fournier et al. (2015). NBC) North Brazil Current, GC) Guiana Current, AO) Amazon River outflow, NECC) North Equatorial Counter Current.

nutrient input. The species composition and biomass distribution is, however, variable across the region and in time, following seasonal changes in Amazon outflow and oceanic currents. After the sediments have settled out, the clear and nutrient-rich surface water allows for massive phytoplankton blooms in the upper 5 m of the water column (Smith and DeMaster, 1996). On the shelf, diatoms, cryptophytes and cyanobacteria draw down most nutrients, whereas in the offshore nitrogen-depleted plume Diatom Diazotroph Associations (DDA) dominate the phytoplankton community (Araujo et al., 2017; Carpenter et al., 1999; Goes et al., 2014; Subramaniam et al., 2008; Yeung et al., 2012). Particularly the DDA are considered to contribute to carbon sequestration from the atmosphere (Yeung et al., 2012). These phytoplankton blooms form the base of the food chain in the otherwise oligotrophic ocean for mesozooplankton of which fecal pellets further enhance carbon export in the WTA (Conroy et al., 2016). Clearly the plume plays a major role in regional ecology as well as net carbon sequestration. However, the onset and establishment of this high primary productivity system is yet unknown. A direct link between the evolution of the transcontinental Amazon River and plume as its oceanic continuum is evident.

The history of the transcontinental Amazon is recorded in the regional ocean floor sediments. Recently, provenance studies on sediments from the Amazon Fan (Hoorn et al., 2017) and Ceará Rise (Van Soelen et al., 2017) date the onset of Andean sediment input in the Atlantic Ocean to ~9.4–9 Ma and ~8.7 Ma, respectively. These new dates bracket the late Miocene age of the onset proposed in studies on the Brazilian Equatorial Margin (BEM) (e.g. Figueiredo et al., 2009, 2010; Gorini et al., 2014) and at Ceará Rise ODP Sites 925 and 926 (Dobson et al., 2001; Harris and Mix, 2002). Sedimentation of both mineral and organic terrigenous material increases slightly during the late Miocene but rises considerably after ~4.5 Ma, following fluvial development and enhanced erosion over the continent, as a result of both Andean uplift and climatic changes during the Plio-Pleistocene (Harris and Mix, 2002; Hoorn et al., 2017; Van Soelen et al., 2017). Moreover, pollen data from the Amazon Fan indicate that a large turnover in the terrestrial environments took place in the Amazon drainage basin during the Neogene. From the Pliocene onwards (< ~4 Ma) grass pollen become more abundant in the Fan sediments, with particularly high percentages in the Pleistocene, which reflect the development of the alpine biome and possibly also the onset of savanna vegetation (Hoorn et al., 2017). In this paper we investigate the marine ecosystem response to increasing fluvial input from the developing Amazon River during the Miocene to Pleistocene.

Marine fossil records provide an opportunity to study the evolution of the marine environmental conditions in relation to Amazon fluvial development. Although diatoms generally dominate phytoplankton communities in the plume at present, diatom silica frustules are not well preserved in the Amazon Fan sediments (Mikkelsen, 1997) due to post-depositional dissolution. Instead, organic and calcareous marine microfossils like dinoflagellate cysts (dinocysts hereafter) and foraminiferal tests are well preserved. Based on present-day distributions distinct ecological preferences of dinocyst taxa (Zonneveld et al., 2013) and foraminifera (Murray, 2006) can be deduced. Their presence and abundance in fossil sediments can therefore be applied as a tool to reconstruct past surface water environmental conditions (dinocysts) and bottom water conditions (benthic foraminifera). Cysts of Protoperidinioid taxa are particularly interesting for this study as they feed on phytoplankton (Jacobson and Anderson, 1986) and are more abundant in areas where primary productivity is high (Zonneveld et al., 2013). Abundance dynamics of Protoperidinioids in fossil assemblages have been successfully applied to reconstruct past primary productivity on various timescales (e.g. Sangiorgi and Donders, 2004; Sluijs et al., 2005; Radi and de Vernal, 2008).

The sediments of the Amazon Fan, located on the BEM (Fig. 1), provide a unique archive of both the river's history and concurrent marine environmental changes. We apply dinocyst and benthic foraminiferal analyses on sediments from 'Well 2' (Figueiredo et al., 2009; Hoorn et al., 2017) to reconstruct marine environmental changes and in particular surface water productivity on the BEM during the Miocene to Pleistocene. In addition, the abundance of terrestrial and freshwater palynomorphs in the sediments is applied as tool to investigate changes in Amazon River input. Planktonic foraminiferal biostratigraphy is performed to support the calcareous nannofossil stratigraphy published in Hoorn et al. (2017). With this multi-proxy approach, we are able to directly link marine environmental changes to fluvial development and continental biome development recorded at the same site (Hoorn et al., 2017). We limit our data interpretations to discussing general trends, aware of the common risk of caving in exploration wells. Nevertheless, the marine microfossils preserved in the record of Well 2 provide first insights into the marine biotic response to the onset and development of the Amazon River.

2. Study area: Amazon Fan

The Amazon submarine fan represents a break in the continental shelf and is situated approximately 400 km north of the Amazon River mouth, in the Foz do Amazonas Basin (Fig. 1). An extensive description of the geological setting is given in Hoorn et al. (2017). Well 2, an exploration well drilled in 2004, is located on the upper section of the Amazon Fan (coordinates: 3° 2′ 58,660″ N, 47° 44′ 45,801″ W) at a water depth of 754 m. Age constraint for this well is provided by high-resolution calcareous nannofossil biostratigraphy (Varol, 2004), which has been updated to GTS2012 (Hoorn et al., 2017). In contrast to sites on the shelf or on deeper parts of the Fan, sedimentation on the upper fan was not interrupted during sea level fluctuations: on the continental shelf almost exclusively sea level highstand deposits are accumulated, whereas in the deep marine extent of the fan mostly lowstand deposits are accumulated (Figueiredo et al., 2009). The well is located near the outer edge of the modern plume year-round (Fig. 1).

For this study sediments from 4692 to 1502 meter below sea level (mbsl) have been analyzed, encompassing the latest Oligocene to Pleistocene period. The lithology for this section of the well is broadly described as an alternation of limestone and mudstone from 4700 to 4080 mbsl, after which siltstone with sandstone bands up to 3620 mbsl and mudstone with a number of silt- and sandstone bands up to 1500 mbsl are present. The well is supported by casings to prevent caving (see depths in lithology Fig. 3). Sedimentation rates in Well 2 increase from ~0.05 m/kyr in the early-mid Miocene to ~0.5 m/kyr after the late Miocene and ~1 m/kyr in the Pleistocene (Hoorn et al., 2017). With exception of hiatuses in the late Miocene (10.8–10.55 Ma),

Table 1
Planktonic and benthic foraminiferal data interpretation for Well 2 studied depths.

Sample details		Planktonic foraminifera (a)		Benthic foraminifera (b)		
depth (mbsl)	age (Ma; GTS2012)	Relevant events	Biostratigraphic zonation	Consistent presence	In association	Interval
1502	0.47					/
1736	0.62			*Bulimina aculeata*	*Nodosaria* sp.	4
2069	0.83			*Bolivina robusta*	*Sphaeroidina bulloides*	4
2159	0.89					4
2249	0.94					/
2492	1.10					/
2645	1.19		N22-N23			4
2663	1.95			*Uvigerina hispida*	*Bulimina marginata*	3
2672	1.97			*Sphaeroidina bulloides*	*Sigmoilopsis schlumbergeri*	3
2708	2.04				*Eponides* sp.	3
2726	2.05	d/s coiling change *G. menardii*			*Cibicides wuellerstorfi*	3
2771	2.17	HO *G. tosaensis*				3
2888	2.40					3
2942	2.45					3
3023	2.50					3
3185	2.61	HO *G. miocenica/ G. extremus*	N21			/
3347	3.72					/
3392	3.81	HO *D. altispira grp*				/
3482	3.99	HO *G. margaritae*				3
3536	4.10					/
3635	4.75	LO *G. miocenica*				/
3709	5.32					/
3714	5.36		N18-N20			/
3720	5.41					/
3726	5.45					/
3744	5.59					/
3756	5.72					/
3780	5.98	HO *Z. nepenthes*				/
3786	6.04	LO *G. tumida*				/
3792	6.10	LO *G. margaritae*				/
3852	6.75					/
3972	8.03					/
4062	8.90	s/d coiling change *G. menardii*				/
4080	9.04					/
4092	9.15		N15-N17			/
4110	9.30					/
4122	9.40	HO *G. dehiscens*				/
4128	9.48	d/s coiling change *N. acostaensis*				/
4158	12.23					/
4164	12.55	HO *G. mayeri/ siakensis*		*Vulvulina pennatula*	*Lenticulina* sp.	2
4182	13.53				*Pyrgo* sp.	/
4200	13.85				*Gyroidina* sp.	/
4224	14.27				*Laticarinina pauperata*	/
4230	14.33		N9-N14		*Globocassidulina subglobosa*	2
4242	14.59				*Uvigerina hispida*	/
4275	15.29				*Amphistegina* sp.	/
4293	15.75	HO *G. dissimilis*			Echinoid spines	2
4344	17.04	HO *G. kugleri*				2
4410	19.04					/
4458	21.05		N4-N8			/
4488	22.32					/
4536	23.02					/
4608	23.42	HO G.ciperoensis		*Pullenia bulloides*	*Oridorsalis tener*	1
4632	23.56			*Sphaeroidina bulloides*	*Globocassidulina subglobosa*	1
4650	23.66	HO G. opima	P23?		*Siphonina* sp.	1
4662	23.73					1
4692	23.89					1

/ no benthics observed in the sampled residue

(continued on next page)

Table 1 (*continued*)

/ indicates sample barren in benthic foraminifera.
[a] Planktonic foraminiferal biostratigraphy based on Blow (1969).
[b] Benthic foraminiferal intervals based on consistently present taxa, additional components for each interval are indicated.

Pliocene (3.7–2.7 Ma) and Pleistocene (1.93–1.2 Ma) Well 2 otherwise represents a generally complete sedimentary record.

3. Methodology

The sample material consisted of cuttings that were primarily collected in siltstone and mudstone lithologies. The dinocysts and foraminifera samplesets overlap by 26 samples and for depths where available material was limited dinocyst and foraminiferal samples are selected in proximity of each other.

3.1. Foraminiferal analyses

A total of 57 samples between 4692 and 1502 mbsl were qualitatively analyzed for planktonic and benthic foraminiferal content (Table 1). Sediment samples of 10 g dry weight were left overnight in a beaker with detergent and distilled water. Subsequently samples were washed over a 63-μm mesh sieve to remove the clay/silt fraction. The residue was dried on a hotplate at 60 °C. The fraction > 125 μm was analyzed qualitatively using a binocular microscope; the 63–125 μm fraction was inspected for rare small-sized specimens. Besides foraminifera, all other elements including ostracods, echinoid spines and coarse mineral grains are recorded.

Planktonic foraminifera are used as a basis for the biostratigraphic zonation (following Blow, 1969; Wade et al., 2011). Due to the effects of caving, mostly highest occurrences (HO) (i.e. extinction events/stratigraphic tops) rather than lowest occurrences (LO) of foraminiferal taxa were considered reliable for age determination. Benthic foraminiferal assemblages are used as indicators for palaeobathymetry and for bottom water conditions (Hayward, 2004; Murray, 2006), in this case oxygenation. Specifically, increased productivity in the surface waters may result in an enhanced organic flux to the seafloor leading to dysoxia (Herguera and Berger, 1991).

Table 2
Palynomorph data for Well 2 studied depths, including subdivision for G-cyst and P-cyst absolute abundances.

Sample details		Palynomorph concentrations (specimen/gr dry weight)							dinocyst counts	
depth (mbsl)	age (Ma; GTS2012)	total palyno-morph	pollen/spores	freshwater algae	acritarchs	dinocysts total	dinocyst Gonyaulacoid	dinocyst Protoperidinioid	total	identified
2609	1.17	937	835	22	27	45	15	29	90	61
2645	1.19	\	\	\	\	\	\	\	barren	\
2663	1.95	1049	947	15	8	52	24	28	115	81
2699	2.02	450	387	2	11	37	18	19	53	40
2726	2.05	\	\	\	\	\	\	\	barren	\
2735	2.10	569	453	7	8	29	14	14	60	46
2825	2.25	\	\	\	\	\	\	\	barren	\
2888	2.40	\	\	\	\	\	\	\	barren	\
2942	2.45	692	629	10	10	29	17	12	65	47
3023	2.50	\	\	\	\	\	\	\	barren	\
3185	2.61	587	495	5	9	53	27	26	97	71
3302	2.68	481	391	8	8	56	38	18	56	45
3347	3.72	436	355	8	15	41	27	14	71	56
3392	3.81	247	192	1	6	34	25	9	109	82
3482	3.99	432	296	11	7	97	86	12	116	104
3536	4.10	\	\	\	\	\	\	\	barren	\
3635	4.75	1420	1225	10	19	162	128	34	100	78
3702	5.27	459	348	5	23	67	40	28	107	83
3714	5.36	\	\	\	\	\	\	\	barren	\
3738	5.54	420	271	5	9	109	92	17	117	106
3756	5.72	347	136	1	4	195	163	33	174	121
3780	5.98	349	160	1	21	157	140	17	117	104
3792	6.10	373	192	0	44	137	108	30	93	68
3906	7.33	330	144	1	3	169	147	22	115	102
3972	8.03	348	105	2	2	212	196	16	119	106
4074	8.99	395	194	0	6	176	140	36	152	136
4092	9.15	68	13	0	1	48	48	0	65	55
4098	9.21	263	48	1	3	103	98	4	119	110
4110	9.30	\	\	\	\	\	\	\	barren	\
4122	9.40	\	\	\	\	\	\	\	barren	\
4134	9.53	\	\	\	\	\	\	\	barren	\
4146	10.89	270	36	0	4	191	188	3	129	113
4164	12.55	267	28	0	5	213	207	6	183	162
4182	13.53	1357	49	0	22	741	730	11	136	133
4194	13.74	656	89	0	10	479	469	10	92	86
4200	13.85	264	37	0	6	214	209	6	116	97
4242	14.59	917	94	3	7	455	367	88	140	123
4293	15.75	728	127	0	0	542	501	41	184	151
4410	19.04	486	108	0	31	330	276	54	116	93

Note: \ indicates sample barren of dinocysts, no further analyses on other palynomorphs is performed.

3.2. Palynological analyses

The palynological content, including organic-walled dinocysts, acritarchs, terrestrial sporomorphs (pollen and spores) and fresh-brackish water algal remains, was quantitatively analyzed in 39 samples from 4410 to 2609 mbsl (Table 2). Chemical processing of the sediment samples was performed at the Laboratory of Paleobotany and Palynology (LPP) in Utrecht NL, and Palynological Laboratory Services Ltd. (PLS), Holyhead UK. Prior to chemical treatment, tablets with a known amount of exotic spores *Lycopodium clavatum* were added to each sample to allow estimation of the sediment palynomorph concentrations. The procedures at both labs included chemical treatment with hydrochloric acid (HCl) and hydrofluoric acid (HF) to remove carbonates and silicates, respectively. Samples were sieved over a 10–15-µm mesh to remove clay and other small particles. The palynological residues were stored in glycerin at the Institute for Biodiversity and Ecosystem Dynamics, Amsterdam.

Homogenized fractions of the palynological residue were mounted on glass slides for analysis using an Olympus light microscope (×400 magnification). We aimed to count at least 100 identified dinocysts per sampled depth, but for poor samples we limited the analysis to a maximum of 3 slides. Samples with < 40 identified dinocysts are omitted, which resulted in the exclusion of 10 of the 39 processed samples for further study (Table 2).

Concentrations of the studied palynomorphs are calculated as number specimens/g dry sediment. As sedimentation rates differ extensively over the sampled interval, palynomorph fluxes (accumulation rates; specimens/cm^{2}y) are also calculated for each sample by multiplying concentration (specimens/g), sedimentation rate (cm/y) and sediment density (g/cm^3) (Appendix A). Sedimentation rates are averaged between age-depth tie-points for each nannozone. Sediment densities are estimated by measuring the weight and volume of 17 sediment samples from different lithological sections.

Taxonomy of the dinocysts follows Fensome (2004), facilitated by the LPP in-house dinocyst library (Palsys.org). Specimens of *Spiniferites* and *Achomosphaera* are grouped into a complex (cpx). Round brown cysts with indications of an archeopyle are grouped as *Brigantedinium* spp., whereas other Protoperidinioid cysts that could not be identified due to damage or folding are grouped as Protoperidinioid indet. Other unidentifiable non-Protoperidinioid dinocysts are grouped as Indet. Dinocyst relative abundances are calculated based on the complete dinocyst sum including unidentified cysts but excluding reworked taxa.

Trends in eukaryotic surface water productivity can be derived from dinocyst assemblages. The ratio between heterotrophic Protoperidinioid (P) and phototrophic Gonyaulacoid (G) dinocysts is frequently used as proxy for primary productivity (P/G ratio; e.g. Sangiorgi and Donders, 2004; Sluijs et al., 2005 and references therein). P/G ratio is calculated by dividing the number of P dinocysts by the total dinocysts counted. As dinocyst counts in a number of samples are low, we calculated 95% confidence intervals for the P-cyst- and total dinocyst concentrations following Maher (1981). The maximal confidence interval (CI) for the P/G ratio is calculated as P-cyst$_{upperCI}$/total dinocyst$_{lowerCI}$ and P-cyst$_{lowerCI}$/total dinocyst$_{upperCI}$. Qualitatively, the level of fluvial input is estimated from the ratio of terrestrial sporomorphs to the total of sporomorphs, marine dinocysts and acritarchs (S/D ratio; Versteegh, 1994), as well as by the presence of fresh-brackish water palynomorphs.

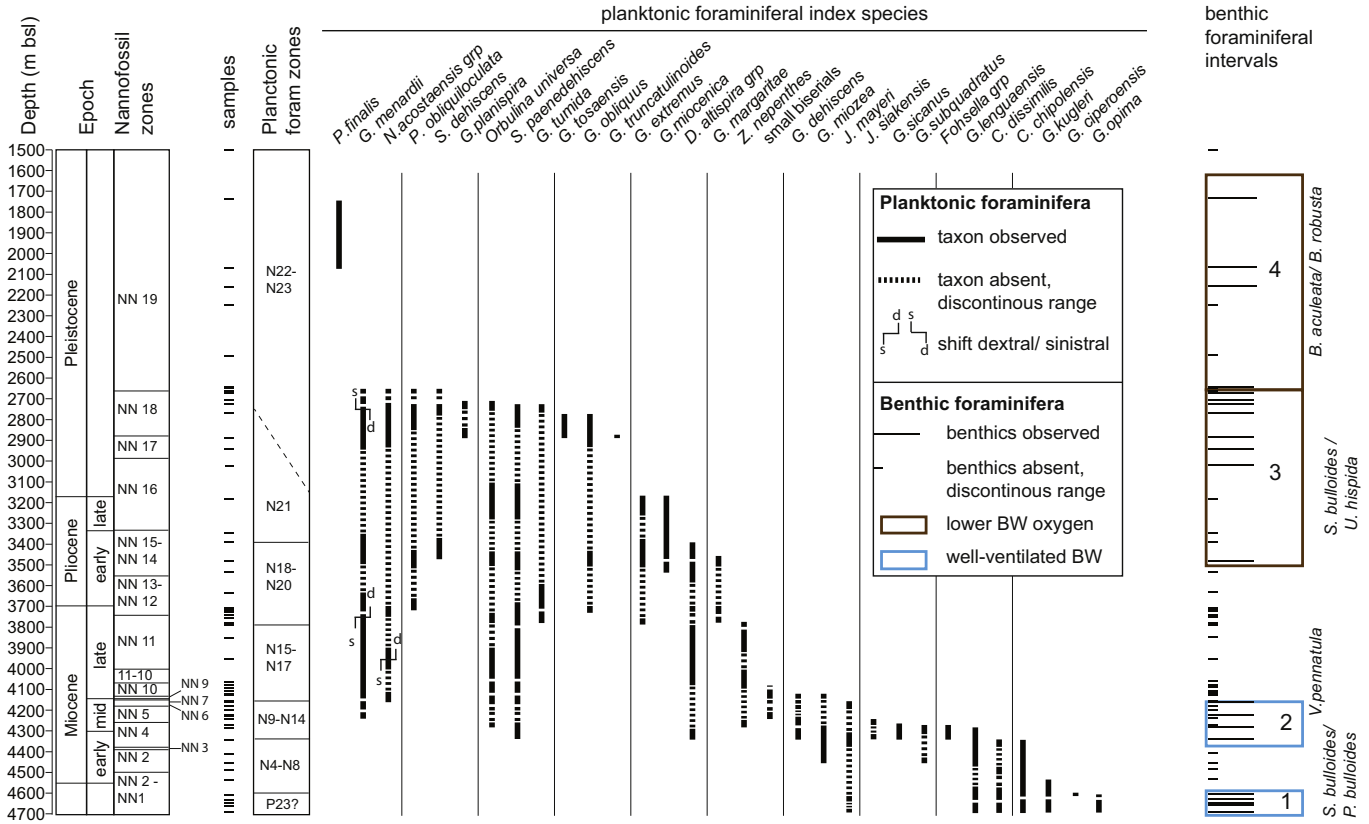

Fig. 2. Well 2 calcareous nannofossil-based age determination as in Hoorn et al. (2017) compared with new planktonic foraminiferal biostratigraphy. Sampled depths for foraminiferal analysis are indicated by horizontal bars. Foraminiferal zonation following (Blow, 1969) is based on highest- and lowest occurrences of planktonic foraminiferal index species (dotted lines indicate discontinuous ranges). Benthic foraminiferal intervals (also discontinuous ranges) are indicated by boxes with main taxa (BW = bottom water).

4. Results and discussion

4.1. Foraminiferal biostratigraphy

Planktonic foraminiferal assemblages are diverse and typically tropical; in total 31 index taxa were identified ranging in age from the latest Oligocene to the Pleistocene (Fig. 2). The first rich assemblages downhole occur at 2708 mbsl and contain *Globorotalia menardii* (sinistral), *Globorotalia planispira* and *Neogloboquadrina acostaensis*, indicative of an early Pleistocene age (N22; Table 1). The Pleistocene-Pliocene boundary is placed between the sinistral/dextral change in coiling direction of the *G. menardii* complex and the HO's of *Globigerinoides extremus* and *Globorotalia miocenica* (2726 and 3185 mbsl). The Miocene-Pliocene boundary can be placed around 3800 mbsl as shown by several datum levels such as the sinistral/dextral change in coiling direction of the *G. menardii* complex, the HO of *Globoquadrina dehiscens* associated with the deepest occurrences of Pliocene markers *Globorotalia tumida* and *Globorotalia margaritae*. The boundary between the early and mid-Miocene in the well is placed at 4285 mbsl based on the HO of the *Praeorbulina* group followed by *Globorotalia lenguaensis* and *Globorotalia kugleri*. Finally, the Oligocene-Miocene boundary based on foraminiferal evidence is placed at 4608 mbsl as indicated by HO's of characteristic species such as *Globorotalia opima* and *Globigerina ciperoensis*. Despite the uncertainties caused by the risk of caving and differences in sampling resolution, the calcareous nannofossil- and planktonic foraminiferal biostratigraphy show a good agreement throughout the studied section (Fig. 2), providing confidence in the nannofossil-based age model for this well (Figueiredo et al., 2009; Hoorn et al., 2017).

4.2. Benthic foraminiferal intervals

Throughout the studied section, benthic foraminifera are generally scarce or absent in the sample residue and the assemblages are generally low diverse (Table 1). Despite the poor and discontinuous presence of benthic foraminifera, four benthic foraminiferal intervals are recognized (Fig. 2). These are from bottom to top: 1) the *Pullenia bulloides/Sphaeroidina bulloides* interval, 2) the *Vulvulina pennatula* interval, 3) the *Uvigerina hispida/Sphaeroidina bulloides* interval and 4) the *Bulimina aculeata/Bolivina robusta* interval (see Table 1 for additional components). Overall, these assemblages indicate a paleo-water depth ranging between 600 and 1000 m at this site during the latest Oligocene to Pleistocene (Murray, 2006), bracketing the present-day water depth of 754 m. Assemblages in interval 1 and 2 are indicative for well-oxygenated bottom water conditions, whereas assemblages in interval 3 and 4 point to increased oxygen deficiency, possibly as a consequence of increased surface water productivity and/or elevated input of organic debris to the ocean floor (Murray, 2006). The benthic foraminifera show distinct changes in faunal composition. However, the overall scarcity in our samples prevents a more robust interpretation of bottom water conditions and explanation of presence/absence throughout the samples in general.

4.3. Overall palynomorph assemblages

A distinct division is visible in the palynomorph composition over the sampled interval (Fig. 3, Table 2): early-mid Miocene samples are dominated by organic-walled dinocysts whereas pollen/spores dominate the Plio-Pleistocene samples. The increasing pollen/spores trend is mimicked by the low but distinct presence of fresh–brackish water algal remains mainly composed of *Pediastrum* and some *Concentricystes/Pseudoschizaea*. Overall, this trend in pollen abundance is comparable to concentration data presented in Hoorn et al. (2017), who interpreted the increase in terrestrial palynomorphs in relation to late Pliocene-Pleistocene climatic variability. More specifically, the increase in herbs, such as grasses and composites, suggests a source area with open

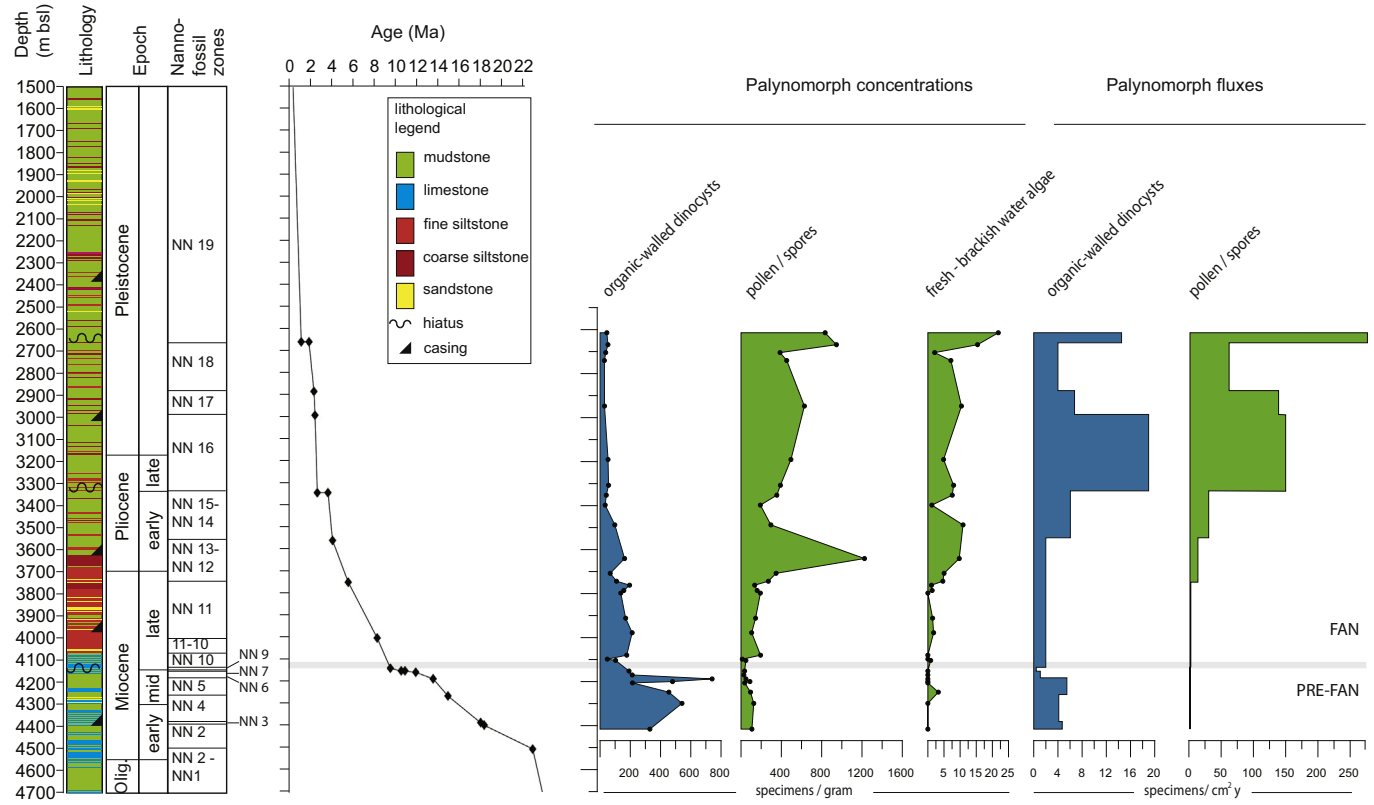

Fig. 3. Overview of Well 2 lithology, age-depth model (Hoorn et al., 2017) and palynomorph absolute abundances. Calculated concentrations of dinocysts, pollen/spores and fresh-brackish water algae, and averaged fluxes of dinocysts and pollen/spores are presented for each sampled nannozone.

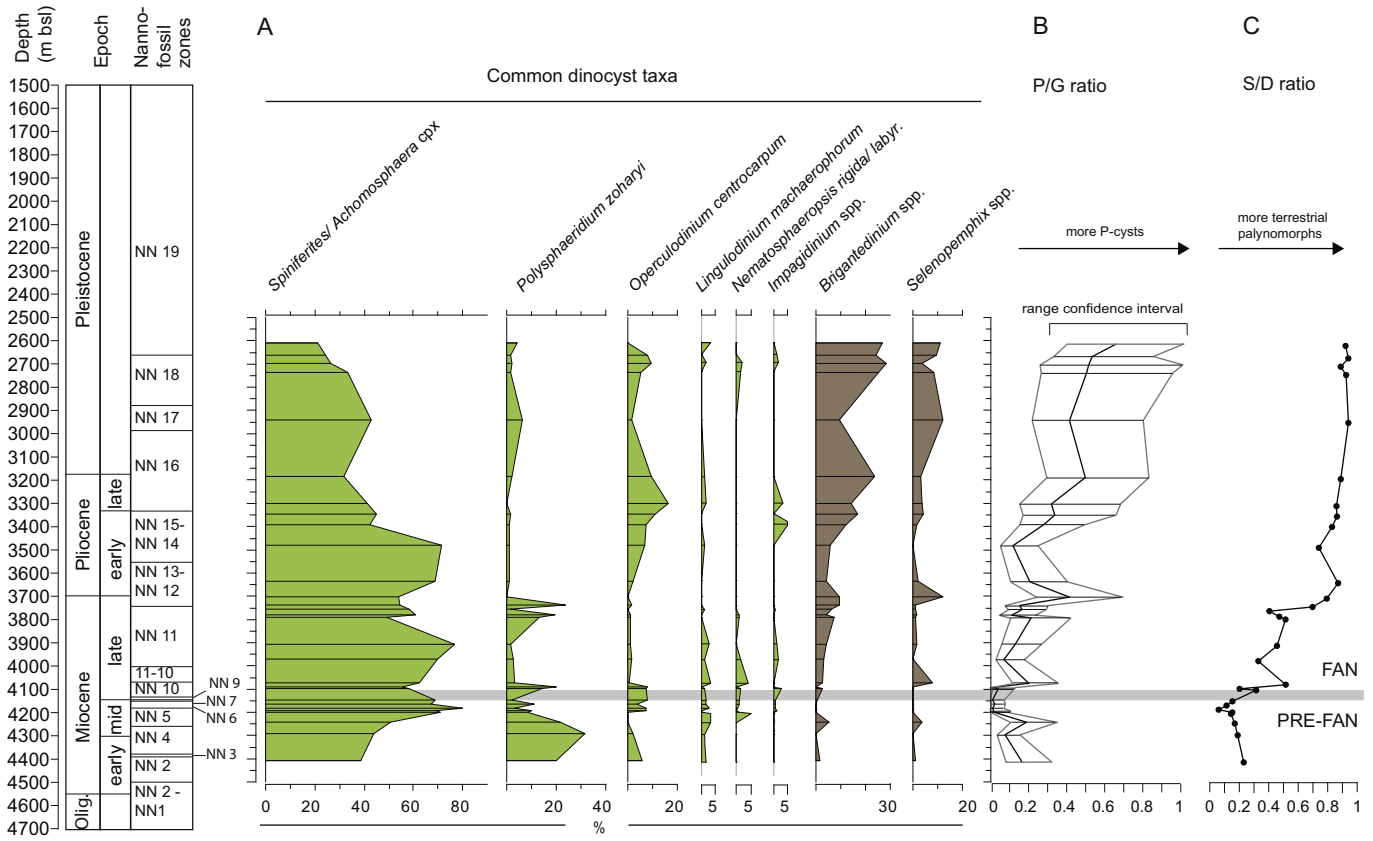

Fig. 4. Relative abundances of selected dinocyst taxa. Green plots indicating Gonyaulacoid taxa and brown indicating Protoperidinioid taxa. P/G ratio (with 95% confidence interval) indicates surface water productivity (see text) and the S/D ratio indicates fluvial input (see text). (For interpretation of the references to colour in this figure legend, the reader is referred to the web version of this article.)

vegetation commonly seen in the high Andes and lowland savannas. Dinocyst concentrations of ~40 cysts/g as found in the Pleistocene samples are much lower than those found in surface samples close to Well 2 on the nutrient-enriched shelf and on the Fan, which vary between 100 and 1000 cysts/g (Vink et al., 2000). As Pleistocene sedimentation rates increase to ~30 times higher than during the early-mid Miocene, the dinocyst flux shows an opposite trend to that of the dinocyst concentrations. The distinctly high flux values during the late Pliocene-Pleistocene are likely an artifact of non-smoothed nannozone-based sedimentation rates than high variation in dinocyst accumulation. Nonetheless, the overall flux trend indicates that low dinocyst absolute abundances in Pleistocene sediments are caused by dilution rather than lower cyst production.

4.4. Dinocyst assemblages

A total of 28 organic-walled dinocyst taxa were identified (Appendix B), but the assemblages are dominated (63–91%) by only five taxa (Fig. 4). Cysts that could not be reliably identified, mostly due to folding or obstruction by amorphous organic particles, make up 18% of the assemblages on average. The early Miocene to early Pliocene sediments are dominated by phototrophic G-cysts belonging to the *Spiniferites/Achomosphaera* complex. At present, different species of *Spiniferites* are globally observed in a wide array of marine biomes (Zonneveld et al., 2013) but are regionally most abundant in the oligotrophic margin of the BEM, outside the influence of the plume (Vink et al., 2000). Distinct peaks of the euryhaline taxon *Polysphaeridium zoharyi* (Zonneveld et al., 2013) occur throughout the Miocene. Nowadays, *P. zoharyi* can dominate in lagoonal surface samples from the Bahama's, northern Gulf of Mexico, Florida and Mexican lagoons samples (Wall et al., 1977; Edwards and Willard, 2001; Limoges et al., 2013). In the early to mid-Miocene peaks of *P. zoharyi* coincide with fragments of echinoids and foraminiferal species *Amphistegina* sp. and *Planorbulina* as observed in the foraminiferal samples, suggesting input from the shelf. Gorini et al. (2014) link distinct buildup phases of the Amazon shelf and fan to 3rd/4th order eustatic sea level variation. Short term sea level drops and consequent transport from the shelf are a plausible mechanism for the observed high abundances of *P. zoharyi* at 5.5–6 Ma, 9.2 Ma, 12.5 Ma and 14.8–18.9 Ma, and which during the late Miocene may also have triggered the connection between the two drainages system of western and eastern Amazonia to form the trans-continental Amazon River (Figueiredo et al., 2009).

During the early Pliocene, the phototrophic cosmopolitan *Operculodinium centrocarpum* as well as heterotrophic Protoperidinioids *Brigantedinium* spp. and *Selenopemphix* spp. distinctly increase. *Brigantedinium* has a global distribution and is considered a cosmopolitan (Zonneveld et al., 2013). Among dinocysts of genus *Selenopemphix*, mostly *S. quanta* and *S. nephroides* are observed; high abundances of *S. quanta* generally occur in river plume areas whereas *S. nephroides* is not commonly observed in river plume areas (Zonneveld et al., 2013). High abundances of Protoperidinioid taxa are commonly observed in the proximity of large river mouths like the Mississippi (Edwards and Willard, 2001; Limoges et al., 2013), the Po (Sangiorgi and Donders, 2004), the Niger (Biffi and Grignani, 1983) and the Congo (Marret, 1994). Moreover, in sediments traps from various sites, a clear positive correlation has been observed between cyst production of *Brigantedinium* plus *Selenopemphix* and biogenic silica fluxes originating from diatom productivity (e.g. Pospelova et al., 2010; Price and Pospelova, 2011). Throughout the record *Nematosphaeropsis* spp. and *Impagidinium* spp., both generally restricted to full-marine environments (Zonneveld et al., 2013) were found in low abundance. *Lingulodinium machaerophorum*, known to thrive in eutrophic conditions, in places where

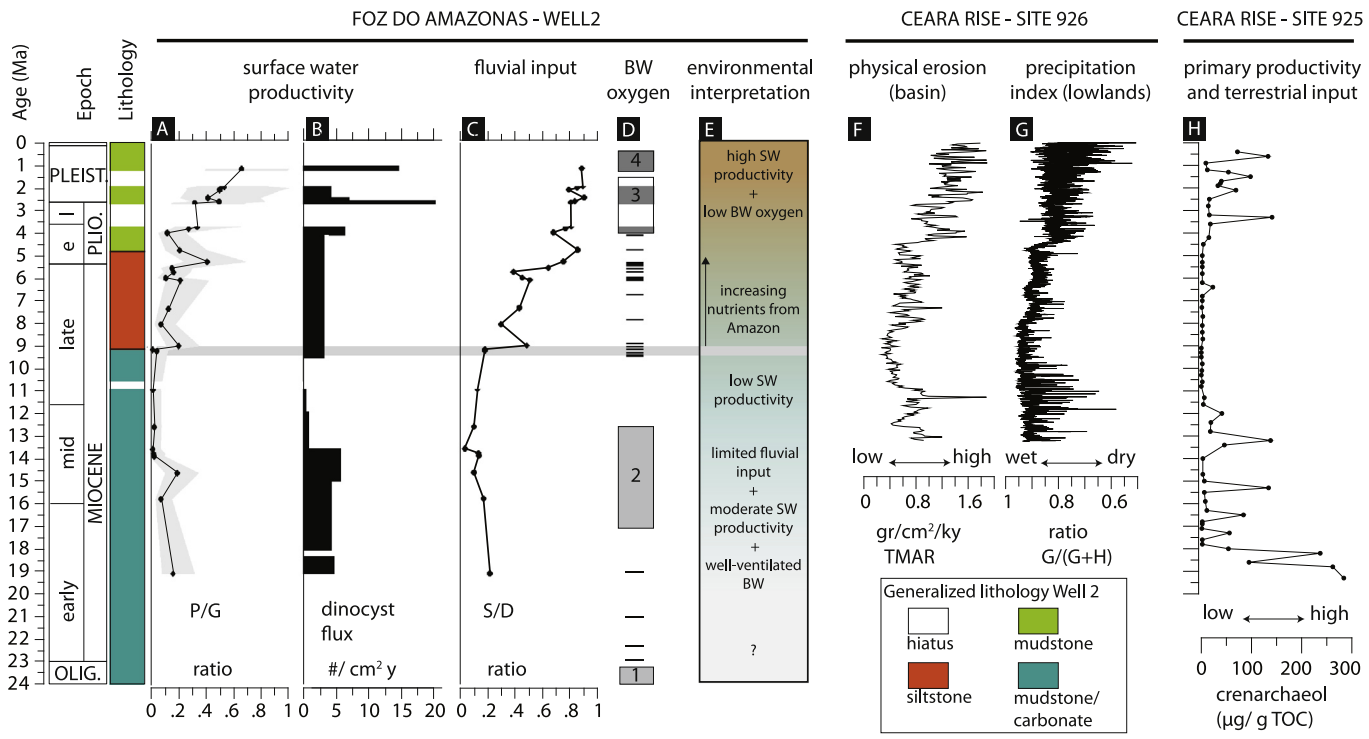

Fig. 5. Overview figure with main changes in Well 2 and ODP Leg 154 Ceará Rise (site 925 and 926) records plotted to age. A) P/G ratio (see text) with confidence interval (grey shading), B) dinocyst fluxes per nannozone, C) S/D ratio (see text), D) benthic foraminiferal intervals (dark shading lower oxygen, light shading high bottom water oxygen). Dots and horizontal lines in plots indicate sampled depths. The horizontal grey bar indicates the approximate onset of the transcontinental Amazon River, following Hoorn et al. (2017). E) Interpretation of environmental changes based on studied proxies (SW = surface water, BW = bottom water). Long-term trends from the margin are compared to geochemistry records of Ceará Rise Site 926 F) terrestrial mass accumulation rates (TMAR) and G) goethite/goethite + hematite ratio as indicator for continental precipitation variability (Harris and Mix, 2002), and Site 925 H) crenarchaeol concentrations as indicator for primary productivity following terrestrial organic material input (Van Soelen et al., 2017).

surface water stratification takes place like near river mouths (Zonneveld et al., 2013), are found but do not show a distinct change over time.

The Pliocene-Pleistocene dinocyst assemblage of Well 2 closely resembles present-day compositions on the margin and slope areas influenced by the plume (Vink et al., 2000). Although relative abundances of extant and fossil assemblages cannot directly be compared due to the presence of extinct taxa in our samples, statistical analyses on the extant regional distribution of dinocysts distinctly place *Spiniferites* spp. and the Protoperidinioids plus *O. centrocarpum* in different groups, being oligotrophic versus eutrophic shelf environment respectively (Vink et al., 2000).

Based on the total dinocyst assemblage, a general increasing trend in the P/G ratio is visible from the late Miocene to the Pleistocene with a distinct rise after the early Pliocene (Fig. 4). This trend is interpreted as an initial minor increase in surface water productivity in the late Miocene, and then a consistent increase from the late Pliocene onwards. We acknowledge that total dinocyst counts are low in some samples (Table 2; Appendix B), however, the trend towards higher P/G ratio values in the Plio-Pleistocene is maintained within the 95% CI. We are therefore confident that the P/G ratio accurately reflects environmental changes. It could be argued that lower bottom water oxygen conditions as reflected by the benthic foraminifera led to better preservation of the oxygen-sensitive P-cysts (Zonneveld et al., 1997), artificially forcing a higher P/G ratio in the Plio-Pleistocene. However, no trend in the level of degradation was observed upon visual inspection in the P-cysts between the high- and low bottom water oxygen samples; specimens of P-cysts in the high bottom water oxygen section during the mid-Miocene were found intact and well-preserved. We therefore deduce that productivity, and not preservation, is the dominant process behind the increasing P/G ratio in the Plio-Pleistocene. Similar to the P/G ratio, the S/D ratio is low during the early to mid-Miocene but increases during the late Miocene and is continuously high from the early Pliocene onwards (Fig. 4). Together with the observed increase in sedimentation rates and presence of fresh-brackish water algae, the S/D pattern is interpreted as indicating high fluvial input from the early Pliocene onwards.

4.5. Amazon-induced productivity in a regional perspective

The combined proxy records suggest the following scenario (Fig. 5A–E): during the early to mid-Miocene surface water conditions at the sampled sites were generally oligotrophic. Limited amounts of terrestrial material from local river system(s) reached the site and the added nutrients likely triggered moderate surface water productivity as reflected in dinocyst taxa composition and fluxes, although not enough to lower bottom water oxygen conditions. From the mid to late Miocene surface water productivity is diminished, until an abrupt shift to increasing fluvial nutrient input and surface water productivity after 9 Ma, coincident with the onset of the transcontinental Amazon River. Terrestrial (in)organic material input increases gradually but from the late Pliocene onwards input is consistently high, triggering peak values in surface water productivity and lower bottom water oxygen conditions. The coinciding trends of both terrestrial (in)organic material input and surface water productivity as reflected in dinocyst taxa composition and fluxes suggest a direct link between the development of the Amazon River and surface water productivity at this site.

To determine whether the distribution of nutrients and sediments reflect a local or regional trend two factors should be considered: oceanic current- and sea level changes. Today, the North Brazil Current (NBC; see Fig. 1) is the motor that transports the nutrient-rich Amazon plume water away from the river mouth northward across the BEM and

past the site of Well 2 (Coles et al., 2013; Hu et al., 2004; Muller-Karger et al., 1988, 1995). The subsequent narrowing and closure of the Central American Seaway during the Neogene led to a reorganization of the Atlantic oceanic currents (e.g. Nisancioglu et al., 2003). With the Central American Seaway still open, the direction of the NBC was southeast, opposite to today. However, Montes et al. (2015) propose that the Panama Isthmus first closed already during the early Miocene. In addition, at Ceará Rise (Site 926, Fig. 1) calcareous dinocyst assemblages indicative for central gyre waters are inferred to show a 'turnover' of the NBC after ~10 Ma (Heinrich and Zonneveld, 2013). This implies that a redirection of oceanic currents could not have caused the trends in sedimentation rates and surface water productivity observed at the BEM during both the late Miocene and Plio-Pleistocene.

Frequent sea level drops of 50–100 m induced by glacial advances during the Plio-Pleistocene (Lisiecki and Raymo, 2005) caused the Amazon River to cut into the largely exposed shelf (Damuth and Kumar, 1975; Gorini et al., 2014). A shoreline more proximal to the site of Well 2 could have resulted in an intensified productivity signal at this site. However, since the birth of the transcontinental Amazon River its fluvial development has also been recorded at Ceará Rise, as indicated by the shift from lowland- to Andean mineral contribution at sites 925 and 926 after 10–8 Ma (Dobson et al., 2001; Harris and Mix, 2002; Van Soelen et al., 2017). Terrestrial mass accumulation rates (TMAR) at Sites 925 (Van Soelen et al., 2017) and 926 (Harris and Mix, 2002 Fig. 5F) show increases after approximately 8.5 Ma and particularly 4.5 Ma that are consistent with the increasing trend in terrestrial palynomorphs input observed in Well 2. Moreover, biomarkers related to terrestrial- and marine-derived organic matter indicate a distinct rise in surface water productivity broadly after 4.5 Ma (Van Soelen et al., 2017; Fig. 5H).

Interestingly, during the early-mid Miocene terrestrial input- and marine primary productivity indicators in both Well 2 and Site 925 (Van Soelen et al., 2017) are elevated, although in Well 2 the trend is not as strong as during the Plio-Pleistocene. This indicates that a river system has been present in this region since at least the early Miocene, well before the transcontinental Amazon River developed (Figueiredo et al., 2009). Furthermore, Gorini et al. (2014) presented seismic evidence from the shelf and upper Fan for a 'proto-Amazon'. Afterwards from ~13–8 Ma dinocyst assemblages and –flux data in Well 2 indicate low productivity and only few terrestrial palynomorphs are found, which is consistent with marine- and terrestrial organic biomarker trends at Site 925 (Van Soelen et al., 2017). At Ceará Rise the sediments representing this period are distinctly different (Dobson et al., 2001; Van Soelen et al., 2017) and contain a chemical composition of a more weathered source (Harris and Mix, 2002), like the local Barreiras Formation or a source on the Brazilian Shield (Figueiredo et al., 2009). This is consistent with coarse fragments of hornblende found in Well 2 foraminiferal samples ranging from ~14–6.5 Ma, which reflect input from a proximal source. Moreover, sedimentation rates at Well 2 are lower during this period. Why the influence of this river system was so distinctly reduced during the latest mid-Miocene and much of the late Miocene should be investigated further. On the other hand, Heinrich and Zonneveld (2013) do find evidence of fluvial input at Site 926 between 11.2 and 9.8 Ma, based on calcareous dinocyst assemblages. Overall, the consistency throughout the Neogene between terrestrial input- and marine productivity records of both the Amazon Fan and the more distant Ceará Rise suggests that our records reflect regional developments.

We relate the observed trends in surface water productivity to the large increment in Andean sediment load that was discharged into the equatorial Western Atlantic by the Amazon River, particularly from Plio-Pleistocene onwards. The cause of this should be sought in the erosion and denudation history of the Andes in relation to Quaternary climatic variability and possibly also the chemical nature of these sediments (Fig. 5G; Harris and Mix, 2002; Hoorn et al., 2017; Van Soelen et al., 2017). The increased terrestrial input rates observed in both the Amazon Fan and Ceará Rise after ~4 Ma are concurrent with increased sediment accumulation rates recorded on, or near, continents across the globe (Molnar, 2004 and references therein). Since this enhanced erosion trend is also observed in basins unaffected by either glaciation or lower sea level, Molnar (2004) argues that an orbitally-forced increase in amplitude and frequency of climatic changes led to enhanced erosion globally. More frequent periods of aridity possibly would have prevented a stable and dense vegetation cover in the Amazon drainage basin, which would explain the increase of grass pollen from late Pliocene onwards (Hoorn et al., 2017) and a consequent more rapid erosion of the unconsolidated sediments of the Amazon lowland. In combination with the erosion of the growing Andes Mountains, nutrient supply to the Atlantic marine environment was likely high during the Plio-Pleistocene, triggering high surface water primary productivity.

5. Conclusions

Our study represents the first marine microfossil multi-proxy approach applied to the sedimentary record of Well 2, a hydrocarbon exploration well in the Foz do Amazonas Basin. It also represents the only record of this nature in the Amazon Fan area for the time interval encompassing the onset and development of the Amazon River system. Based on our multi-proxy records the following scenario can be drawn: during the early to early-late Miocene alternating clays and carbonates were deposited at the BEM under surface water conditions that sustain low to moderate surface water productivity. Occasional pulses of fluvial input from local river systems occurred. Benthic foraminifera indicate well-oxygenated bottom water conditions. After ~9 Ma, with the breakthrough of the transcontinental Amazon River, terrestrial derived (in)organic material is delivered to the ocean with increasing rates. The abundance of primary productivity indicators rises simultaneously with fluvial input suggesting a direct link between Amazon River development and high surface water productivity in the Plio-Pleistocene. Although the benthic foraminiferal record is erratic, it indicates a general dysoxic environment during this period. The temporal consistency between records from the Amazon Fan and the more distant Ceará Rise reflect large-scale marine environmental changes followed the development of the Amazon River, likely related to increased climatic variability in the Amazon Basin during the Plio-Pleistocene.

Supplementary data to this article can be found online at https://doi.org/10.1016/j.palaeo.2018.05.048.

Acknowledgments

We acknowledge the Brazilian Oil and Gas Agency (ANP) for allowing us to publish selected 1-BP-3 APS well data (Well 2, following Figueiredo et al., 2009, and Hoorn et al., 2017). Funding: CLIM-AMAZON European Union's Seventh Framework Program (FP7/2007-2013) and the Universidade de Brasília funded E.L. (grant 295091) and facilitated this project. We greatly thank Natasja Welters for sample processing, Suzette Flantua for constructing the map, Roberto D'Avila, Emilson Soares, Osman Varol, Stephen Lowe, David Pocknall, Ricardo Pinto, Els van Soelen and Peter Bijl for constructive discussions, and Jorge Figueiredo and Paulus van der Ven for initiating the cooperation Petrobras-UvA.

References

Araujo, M., Noriega, C., Hounsou-gbo, G.A., Veleda, D., Araujo, J., Bruto, L., ... Otsuka, A., 2017. A synoptic assessment of the Amazon River-ocean continuum during boreal autumn: from physics to plankton communities and carbon flux. Front. Microbiol. 8, 1358.

Biffi, U., Grignani, D., 1983. Peridinioid dinoflagellate cysts from the Oligocene of the Niger Delta, Nigeria. Micropaleontology 29, 126–145.

Blow, W.H., 1969. Late Middle Eocene to Recent planktonic foraminiferal biostratigraphy. In: Proceedings of the First International Conference on Planktonic Microfossils. vol. 1. EJ Brill, Leiden, pp. 199–422.

Carpenter, E.J., Montoya, J.P., Burns, J., Mulholland, M.R., Subramaniam, A., Capone,

D.G., 1999. Extensive bloom of a N 2-fixing diatom/cyanobacterial association in the tropical Atlantic Ocean. Mar. Ecol. Prog. Ser. 273–283.
Coles, V.J., Brooks, M.T., Hopkins, J., Stukel, M.R., Yager, P.L., Hood, R.R., 2013. The pathways and properties of the Amazon River Plume in the tropical North Atlantic Ocean. J. Geophys. Res. Oceans 118 (12), 6894–6913.
Conroy, B.J., Steinberg, D.K., Stukel, M.R., Goes, J.I., Coles, V.J., 2016. Meso-and microzooplankton grazing in the Amazon River plume and western tropical North Atlantic. Limnol. Oceanogr. 61 (3), 825–840.
Dai, A., Trenberth, K.E., 2002. Estimates of freshwater discharge from continents: latitudinal and seasonal variations. J. Hydrometeorol. 3 (6), 660–687.
Damuth, J.E., Kumar, N., 1975. Amazon Cone: morphology, sediments, age, and growth pattern. Geol. Soc. Am. Bull. 86 (6), 863–878.
Del Vecchio, R., Subramaniam, A., 2004. Influence of the Amazon River on the surface optical properties of the western tropical North Atlantic Ocean. J. Geophys. Res. Oceans 109 (C11).
Dobson, D.M., Dickens, G.R., Rea, D.K., 2001. Terrigenous sediment on Ceara Rise: a Cenozoic record of South American orogeny and erosion. Palaeogeogr. Palaeoclimatol. Palaeoecol. 165 (3), 215–229.
Edwards, L.E., Willard, D.A., 2001. Dinoflagellate cysts and pollen from sediment samples, Mississippi Sound and Gulf of Mexico. In: Stratigraphic Framework of the Neogene and Quaternary Sediments of the Mississippi Coastal Zone, Jackson County, Mississippi. US Geological Survey Open-file Report, 01-415.
Fensome, R.A., 2004. The Lentin and Williams Index of Fossil Dinoflagellages (Contribution Series Number 42). American Association of Stratigraphic Palynologists Foundation, Dallas, TX.
Figueiredo, J.J.J.P., Hoorn, C., Van der Ven, P., Soares, E., 2009. Late Miocene onset of the Amazon River and the Amazon deep-sea fan: evidence from the Foz do Amazonas Basin. Geology 37 (7), 619–622.
Figueiredo, J.J.J.P., Hoorn, C., Van der Ven, P., Soares, E., 2010. Late Miocene onset of the Amazon River and the Amazon deep-sea fan: evidence from the Foz do Amazonas Basin: reply. Geology 38 (7), e213.
Fournier, S., Chapron, B., Salisbury, J., Vandemark, D., Reul, N., 2015. Comparison of spaceborne measurements of sea surface salinity and colored detrital matter in the Amazon plume. J. Geophys. Res. Oceans 120 (5), 3177–3192.
Goes, J.I., do Rosario Gomes, H., Chekalyuk, A.M., Carpenter, E.J., Montoya, J.P., Coles, V.J., ... Steinberg, D.K., 2014. Influence of the Amazon River discharge on the biogeography of phytoplankton communities in the western tropical north Atlantic. Prog. Oceanogr. 120, 29–40.
Gorini, C., Haq, B.U., dos Reis, A.T., Silva, C.G., Cruz, A., Soares, E., Grangeon, D., 2014. Late Neogene sequence stratigraphic evolution of the Foz do Amazonas Basin, Brazil. Terra Nova 26 (3), 179–185.
Harris, S.E., Mix, A.C., 2002. Climate and tectonic influences on continental erosion of tropical South America, 0–13 Ma. Geology 30 (5), 447–450.
Hayward, B.W., 2004. Foraminifera-based estimates of paleobathymetry using Modern Analogue Technique, and the subsidence history of the early Miocene Waitemata Basin. N. Z. J. Geol. Geophys. 47 (4), 749–767.
Heinrich, S., Zonneveld, K.A.F., 2013. Influence of the Amazon River development and constriction of the Central American Seaway on Middle/Late Miocene oceanic conditions at the Ceara Rise. Palaeogeogr. Palaeoclimatol. Palaeoecol. 386, 599–606.
Herguera, J.C., Berger, W., 1991. Paleoproductivity from benthic foraminifera abundance: glacial to postglacial change in the west-equatorial Pacific. Geology 19 (12), 1173–1176.
Hoorn, C., Bogotá-A, G.R., Romero-Baez, M., Lammertsma, E.I., Flantua, S.G., Dantas, E.L., ... Chemale, F., 2017. The Amazon at sea: onset and stages of the Amazon River from a marine record, with special reference to Neogene plant turnover in the drainage basin. Glob. Planet. Chang. 153, 51–65.
Hu, C., Montgomery, E.T., Schmitt, R.W., Muller-Karger, F.E., 2004. The dispersal of the Amazon and Orinoco River water in the tropical Atlantic and Caribbean Sea: observation from space and S-PALACE floats. Deep-Sea Res. II Top. Stud. Oceanogr. 51 (10), 1151–1171.
Jacobson, D.M., Anderson, D.M., 1986. Thecate heterophic dinoflagellates: feeding behavior and mechanisms. J. Phycol. 22 (3), 249–258.
Körtzinger, A., 2003. A significant CO_2 sink in the tropical Atlantic Ocean associated with the Amazon River plume. Geophys. Res. Lett. 30 (24).
Limoges, A., Londeix, L., de Vernal, A., 2013. Organic-walled dinoflagellate cyst distribution in the Gulf of Mexico. Mar. Micropaleontol. 102, 51–68.
Lisiecki, L.E., Raymo, M.E., 2005. A Pliocene-Pleistocene stack of 57 globally distributed benthic $\delta^{18}O$ records. Paleoceanography 20 (1).
Maher, L.J., 1981. Statistics for microfossil concentration measurements employing samples spiked with marker grains. Rev. Palaeobot. Palynol. 32 (2–3), 153–191.
Marret, F., 1994. Distribution of dinoflagellate cysts in recent marine sediments from the east Equatorial Atlantic (Gulf of Guinea). Rev. Palaeobot. Palynol. 84 (1–2), 1–22.
Mikkelsen, N., 1997. Upper Quaternary diatoms in the Amazon Fan of the western Atlantic. In: Flood, R.D., Piper, D.J.W., Klaus, A., Peterson, L.C. (Eds.), Proceedings of the Ocean Drilling Program, Scientific Results. vol. 155.
Molnar, P., 2004. Late Cenozoic increase in accumulation rates of terrestrial sediment: how might climate change have affected erosion rates? Annu. Rev. Earth Planet. Sci. 32, 67–89.
Montes, C., Cardona, A., Jaramillo, C., Pardo, A., Silva, J.C., Valencia, V., Ayala, C., Pérez-Angel, L.C., Rodriguez-Parra, L.A., Niño, H., 2015. Middle Miocene closure of the Central American seaway. Science 348 (6231), 226–229.
Muller-Karger, F.E., McClain, C.R., Richardson, P.L., 1988. The dispersal of the Amazon's water. Nature 333 (6168), 56–59.
Muller-Karger, F.E., Richardson, P.L., McGillicuddy, D., 1995. On the offshore dispersal of the Amazon's plume in the North Atlantic: comments on the paper by A. Longhurst, “Seasonal cooling and blooming in tropical oceans”. Deep-Sea Res. I Oceanogr. Res. Pap. 42 (11), 2127–2137.
Murray, J.W., 2006. Ecology and Applications of Benthic Foraminifera. Cambridge University Press.
Nisancioglu, K.H., Raymo, M.E., Stone, P.H., 2003. Reorganization of Miocene deep water circulation in response to the shoaling of the Central American Seaway. Paleoceanography 18 (1).
Pospelova, V., Esenkulova, S., Johannessen, S.C., O'Brien, M.C., Macdonald, R.W., 2010. Organic-walled dinoflagellate cyst production, composition and flux from 1996 to 1998 in the central Strait of Georgia (BC, Canada): a sediment trap study. Mar. Micropaleontol. 75 (1), 17–37.
Price, A.M., Pospelova, V., 2011. High-resolution sediment trap study of organic-walled dinoflagellate cyst production and biogenic silica flux in Saanich Inlet (BC, Canada). Mar. Micropaleontol. 80 (1), 18–43.
Radi, T., de Vernal, A., 2008. Dinocysts as proxy of primary productivity in mid–high latitudes of the Northern Hemisphere. Mar. Micropaleontol. 68 (1–2), 84–114.
Salisbury, J., Vandemark, D., Campbell, J., Hunt, C., Wisser, D., Reul, N., Chapron, B., 2011. Spatial and temporal coherence between Amazon River discharge, salinity, and light absorption by colored organic carbon in western tropical Atlantic surface waters. J. Geophys. Res. Oceans 116 (C7).
Sangiorgi, F., Donders, T.H., 2004. Reconstructing 150 years of eutrophication in the north-western Adriatic Sea (Italy) using dinoflagellate cysts, pollen and spores. Estuar. Coast. Shelf Sci. 60 (1), 69–79.
Sluijs, A., Pross, J., Brinkhuis, H., 2005. From greenhouse to icehouse; organic-walled dinoflagellate cysts as paleoenvironmental indicators in the Paleogene. Earth Sci. Rev. 68 (3), 281–315.
Smith, W.O., Demaster, D.J., 1996. Phytoplankton biomass and productivity in the Amazon River plume: correlation with seasonal river discharge. Cont. Shelf Res. 16 (3), 291–319.
Subramaniam, A., Yager, P.L., Carpenter, E.J., Mahaffey, C., Björkman, K., Cooley, S., Kustka, A., Montoya, J.P., Sañudo-Wilhelmy, S.A., Shipe, R.F., Capone, D.G., 2008. Amazon River enhances diazotrophy and carbon sequestration in the tropical North Atlantic Ocean. Proc. Natl. Acad. Sci. 105 (30), 10460–10465.
Van Soelen, E.E., Kim, J.H., Santos, R.V., Dantas, E.L., de Almeida, F.V., Pires, J.P., ... Damsté, J.S.S., 2017. A 30 Ma history of the Amazon River inferred from terrigenous sediments and organic matter on the Ceará Rise. Earth Planet. Sci. Lett. 474, 40–48.
Varol Research, 2004. Nannofossil Biostratigraphy of BP Offshore Well. Internal Report. Agência Nacional do Petróleo, Gás Natural e Biocombustíveis, Brazil.
Versteegh, G.J.M., 1994. Recognition of cyclic and non-cyclic environmental changes in the Mediterranean Pliocene: a palynological approach. Mar. Micropaleontol. 23 (2), 147–183.
Vink, A., Zonneveld, K.A., Willems, H., 2000. Organic-walled dinoflagellate cysts in western equatorial Atlantic surface sediments: distributions and their relation to environment. Rev. Palaeobot. Palynol. 112 (4), 247–286.
Wade, B.S., Pearson, P.N., Berggren, W.A., Pälike, H., 2011. Review and revision of Cenozoic tropical planktonic foraminiferal biostratigraphy and calibration to the geomagnetic polarity and astronomical time scale. Earth Sci. Rev. 104 (1), 111–142.
Wall, D., Dale, B., Lohmann, G.P., Smith, W.K., 1977. The environmental and climatic distribution of dinoflagellate cysts in modern marine sediments from regions in the North and South Atlantic Oceans and adjacent seas. Mar. Micropaleontol. 2, 121–200.
Yeung, L.Y., Berelson, W.M., Young, E.D., Prokopenko, M.G., Rollins, N., Coles, V.J., Montoya, J.P., Carpenter, E.J., Steinberg, D.K., Foster, R.A., Capone, D.G., Yager, P.L., 2012. Impact of diatom-diazotroph associations on carbon export in the Amazon River plume. Geophys. Res. Lett. 39 (18).
Zonneveld, K.A., Versteegh, G.J., de Lange, G.J., 1997. Preservation of organic-walled dinoflagellate cysts in different oxygen regimes: a 10,000 year natural experiment. Mar. Micropaleontol. 29 (3–4), 393–405.
Zonneveld, K.A., Marret, F., Versteegh, G.J., Bogus, K., Bonnet, S., Bouimetarhan, I., ... Esper, O., 2013. Atlas of modern dinoflagellate cyst distribution based on 2405 data points. Rev. Palaeobot. Palynol. 191, 1–197.